



ELSEVIER

Contents lists available at ScienceDirect

Nuclear Instruments and Methods in Physics Research A

journal homepage: www.elsevier.com/locate/nima

RF properties of a X-band hybrid photoinjector

B. Spataro^c, A. Valloni^{a,b,*}, D. Alesini^c, N. Biancacci^a, L. Faillace^d, L. Ficcadenti^c, A. Fukusawa^b, L. Lancia^a, M. Migliorati^a, F. Morelli^a, A. Mostacci^a, B. O'Shea^b, L. Palumbo^a, J.B. Rosenzweig^b, A. Yakub^b

^a Dipartimento di Scienze di Base e Applicate per l'Ingegneria, Universita' degli Studi di Roma "La Sapienza", Via Antonio Scarpa 14, Roma (RM) 00185, Italy

^b UCLA Dept. of Physics and Astronomy, 405 Hilgard Ave., Los Angeles, CA 90095, USA

^c Istituto Nazionale di Fisica Nucleare—Laboratori Nazionali di Frascati, via Enrico Fermi 40, Frascati (RM), Italy

^d RadiaBeam Technologies, LLC, 1717 Stewart Ave., Santa Monica, CA 90404, USA

ARTICLE INFO

Available online 7 May 2011

Keywords:

Hybrid photoinjector

X-band

RF design

ABSTRACT

An INFN-LNF/UCLA/SAPIENZA collaboration is developing a hybrid photoinjector in X-band. A hybrid photoinjector is a novel high brightness electron source that couples a standing wave cell cavity (acting as an RF gun) directly to a multi-cell travelling-wave structure. This configuration offers a number of advantages over the split standing wave/travelling-wave system. Most notably the reflected RF transient is almost completely suppressed, thus eliminating the need for a circulator and the bunch lengthening effect that occurs in the drift section of the split system. These properties allow scaling of the device to higher field and frequencies, which should dramatically improve beam brightness. The RF coupling between the standing and the traveling wave sections is accomplished in the fourth cell encountered by the beam, with the SW section electrically coupled to it on-axis. This mode of coupling is particularly advantageous, as it is accompanied by a 90° phase shift in the accelerating field, resulting in strong velocity bunching effects on the beam that reverse the usual bunch lengthening induced after the gun exit in standard 1.6 cell photoinjectors. In this scenario, from the beam dynamics point of view, it is seen that device may produce ten's of femtosecond beams at ~3.5 MeV and the emittance compensation dynamics remains manageable even in the presence of strong compression. We present here a survey of the device characteristics. In particular we show the results of the electromagnetic simulations, a beam dynamics analysis related to the temperature tuning of the SW and TW section, and a RF characterization using bead pull and scattering coefficient measurements of a device prototype.

© 2011 Elsevier B.V. All rights reserved.

1. Introduction

Recent years have seen a revolution in the production of high brightness electron beams because of the maturation of RF photoinjector performance. This maturation derives its genesis from a multi-disciplinary approach to the difficult problems presented to by understanding the behaviour of an electron beam under the combined influence of large external applied electromagnetic fields and the self-induced space charge fields. Through these theoretical, computational and experimental investigations, photoinjector physics has established itself at the confluence of a large number of disciplines, including accelerator beam dynamics, plasma physics, large-scale computational physics, surface studies, high-field RF physics and laser engineering. The

manifest success of the RF photoinjectors is a testament to this collective understanding.

The most prevalent photoinjector design in use today employs an arrangement of two accelerating structures, a 1.5/1.6 SW gun and a post accelerating section. This scheme presents some inconveniences. The two structures are fed independently and, since the SW structure reflects nearly all of the input power at the beginning of the RF filling process, circulators and isolators are needed in order to protect the RF power source. In addition, scaling the fields of the split system into X-band is not possible due to high electric fields that could exceed the RF breakdown limitations. In order to circumvent these and other limitations in existing photoinjector designs we present a hybrid configuration that consists of one accelerating structure where the TW and the SW parts are tightly axially coupled. The model of the hybrid structure is shown in Fig. 1. In particular the hybrid photoinjector uses a coupling cell to divide power between a high gradient standing wave section for electron emission and collection, and a lower gradient travelling wave accelerator for acceleration to

* Corresponding author at: Dipartimento di Scienze di Base e Applicate per l'Ingegneria, Universita' degli Studi di Roma "La Sapienza", Via Antonio Scarpa 14, Roma (RM) 00185, Italy. Tel.: + 00393291809698.

E-mail address: alessandra.valloni@uniroma1.it (A. Valloni).

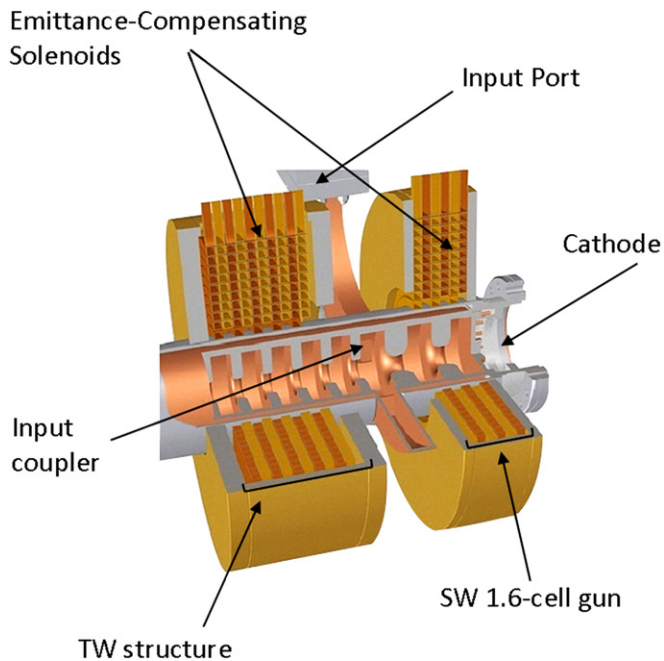


Fig. 1. 3D drawing of the compact hybrid structure showing the relevant parts of the device. It begins at the upstream end with the SW RF gun section in the initial cells (1.6 cell gun in this model), which is coupled to the RF power that is fed from the waveguide into the structure through a traveling wave coupling cell. Emittance-compensating solenoid are included.

desired energies at low emittances. This novel design strongly mitigates the RF reflection problem as the SW section represents a small fraction ($\sim 10\%$) of the input power, and the existence of the TW section permits near complete matching to the input waveguide. Thus, one can omit the circulator that a SW RF gun generally requires. This feature enables one to build a photoinjector at X-band frequencies, where no circulators, with the relevant high powers, yet exist. To provide an initial summary, therefore, the main advantages of this class of devices are that:

- they mitigate impedance mismatches, and therefore reflected RF power, both during and after the RF filling and turnoff of the SW section; the almost complete removal of the transient RF reflected power allows scaling to high frequency;
- they require a much simpler high power RF system than a split photoinjector; there is only one klystron and multiple waveguide sections, attenuators, and phase shifters are avoided;
- they are more compact than a split system;
- the acceleration dynamics is robust, this indicates flexibility in operating energy by simply changing RF power and laser injection parameters;
- they avoid the bunch lengthening observed during the drift in a split photoinjector;

they actually strongly longitudinally focus through velocity bunching, due to the phase shift between SW cell and input coupler. For example in this paper we will show that for a X-band device (with typical peak field of 200 MV/m) the emittance compensation dynamics remain manageable even in the presence of strong compression and ten's of femtosecond high brightness beams are deliverable at ~ 3.5 MeV. The current initiative in X-band follows that of a S-band hybrid gun, now under construction at LNF and with high power testing/beam production measurements foreseen at UCLA. This S-band hybrid has 1.55 SW cells and 9 TW cells, and it produces strongly compressed 3.5 MeV beam. It can be optionally used with a 3 m TW linac fed

from RF output of the hybrid, to boost the energy up to 22 MeV. This device works at 2.856 GHz and presents 60 MV/m of peak field in the SW section and an average field in the TW cells of 13.5 MV/m [1a,1b]. The design strategy of the X-band hybrid photoinjector that we implemented started from scaling the S-band model to the X-band. The RF electric field and the external focusing magnetic field are scaled by a factor 4 in agreement with the scaling laws ($E \propto \lambda^{-1}$ and $B \propto \lambda^{-1}$ [2]). While scaling the design is conceptually simple, practical limits require some changes in both RF and magnetostatic designs. In accordance with the scaling principles applied to the current S-band hybrid structure, the X-band hybrid had initially a 1.6 cell SW part. On this structure at the same time beam dynamics studies and electromagnetic analysis were performed in order to optimize its performances. Afterwards a prototype has been built and measured in order to better understand the device potentialities and the manufacturing difficulties. Then the number of cells of the SW gun section was increased to 2.6 for two specific reasons: to reach higher energy at the gun exit, and to have more space available for focusing magnets, which relaxes the challenge of scaling the magnetic field appropriately. This class of photoinjectors offers a wide variety of applications ranging from multi-THz coherent radiation production to ultra-fast electron diffraction. Relevant details of the applications, as well as considerable further details concerning the beam dynamics in the device, are included in a companion paper [3]. In the following sections of this paper we first illustrate the general procedure to design the hybrid structure. In particular we discuss the results of the electromagnetic simulations obtained with the code HFSS [4] and the main beam dynamics properties. In the following part of the paper we show the electric field measurements using bead pull technique that validate the electromagnetic design produced with simulation.

2. RF design

The device can be conceptually divided into two main parts, *i.e.* the SW and the TW sections. These two parts can be initially designed separately by 2D or 3D general purpose electromagnetic codes solving the Maxwell equations in the structure. One can simulate the two sub-structures separately assuming a perfect magnetic plane in the centre of the coupling iris in order to force the field solution to have the vanishing longitudinal electric field, which is physically sound. The SW cells radius and the iris dimensions are chosen to achieve the proper resonant frequency, the mode separation and a constant maximum field in the cells (the so called field flatness), while the length of the SW cell is chosen to impose a π -mode. The design of the TW section starts considering the single TW cell and deriving the cell radius and length. The requirement is that the TM_{010} -like mode propagates with a phase advance per cell of 120° at the working frequency, *i.e.* the resonant frequency of the SW part (11.424 GHz). This operation mode is found by modeling planes of periodicity (*i.e.* master-slave boundary conditions on the cell walls), where the E -field on one surface matches the E -field on another with the desired phase difference. The radius of the input/output coupling cells (*e.g.* the input coupler shown in Fig. 1) and the dimension of the hole coupling the feeding waveguide are chosen to meet the request of small reflection at the input port (as in conventional TW structures). The design technique (namely the short circuit method) is based on a simple circuit representation in where each cell of the TW structure is modelled by a two port network; the coupling cell (*i.e.* the cell matching the input/output waveguide to the disc loaded structure) is described with a two port scattering matrix as well. The phase of the reflection coefficient at the input

the condition that is always fulfilled in the hybrid gun. To validate this result we compared HFSS simulations of the whole structure with the approximate model have been compared obtaining a good agreement among them [8]. As anticipated above, the coupling iris diameter allows adjustment of the ratio $E_{z,p,SW}/\langle E_{z,TW} \rangle$: in particular if we increase the diameter we increase this ratio and for a coupling iris radius $a_c=2.7$ mm we obtain a ratio of 4.1. Making a sensitivity analysis with respect to the radius of the coupling iris

and varying it in the range of 2.2–3 mm, we observe that $E_{z,p,SW}/\langle E_{z,TW} \rangle$ varies linearly with a_c in the range of 2.5–3 mm, whereas for values lower than 2.2 mm the ratio is almost constant, indicating a lack of coupling between gun and coupler. The reflection coefficient shown in Fig. 4, at the input port of the structure is lower than 20 dB. In the same plot the transmission coefficient between the gun probe and the waveguide input port is also reported. This 90° phase jump is not ideal for optimal acceleration,

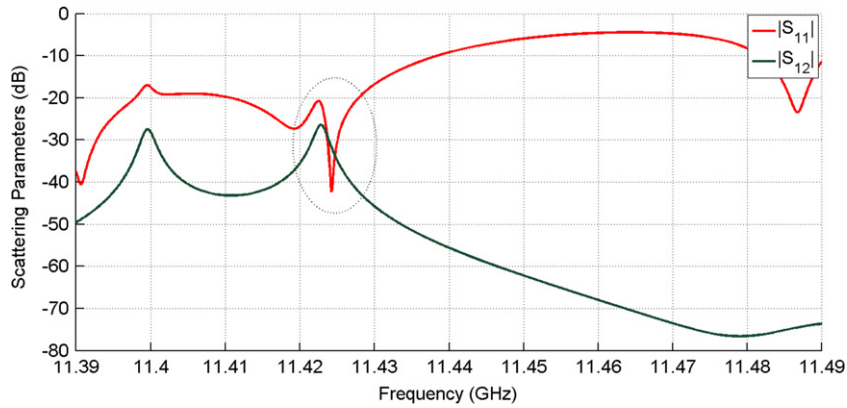
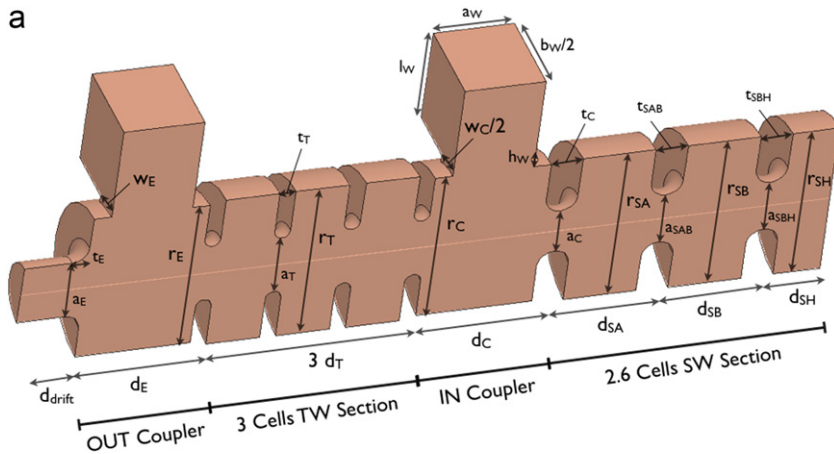


Fig. 4. S_{11} at the waveguide input port and S_{21} between the gun probe and the waveguide input port.



b

Parameter	Value [mm]	Parameter	Value [mm]
r_{SA}	10.511	d_T	8.747
r_{SB}	10.537	a_{SAB}, a_{SBH}	3.5
r_{SH}	10.436	a_T, a_E	4
a_C	3	t_{SAB}, t_{SBH}	4
r_C	10.17	t_C	4.76
w_C	8.131	t_T, t_E	2
r_E	10.168	a_w	10.16
w_E	8.073	b_w	22.86
d_{SH}	7.872	l_w	12.5
d_{SA}, d_{SB}	13.12	h_w	0.15
d_C, d_E	17.494	d_{drift}	6

Fig. 5. 3D model of the hybrid structure simulated with HFSS. The scheme is characterized by 2.6 cell SW gun and 3 cell TW section.

but it is instead useful for velocity bunching that allows obtaining very high current and low emittance beams. Since the phase of the longitudinal electric field between the SW gun and the TW section is almost fixed, the accelerating field and the beam can be synchronized by properly by choosing the length of the input coupler cell and the injection phase. In particular, with an un-naturally long coupling cell of $2\lambda/3$ the beam enters to the TW section exactly on the crest. With the natural choice of cell length $5\lambda/12$ (i.e. half of a π -mode SW and half of a $2\pi/3$ -mode TW cell) the bunch enters to the TW section on the slope of the E_z and it can be longitudinally compressed using the velocity bunching technique. We define the first option continuous acceleration (CA) and the second one velocity bunching acceleration (VB). The model here presented has a coupler length of $2/3\lambda$ with $\lambda=26.24$ mm, obtained considering that if a

particle experiences in the full standing cell a maximum value of electric field, the flight time to reach the first cell of the travelling cell has to be exactly the right time to see another maximum of field (CA mode). Then one can play with the injection phase in order to conveniently synchronize the beam with the electric field. As stated above, due to the applications investigated, the number of cells of the SW gun is increased to 2.6 in order to obtain higher values of energy at the gun exit, as one is constrained to operate at X-band with a small normalized electric field $eE/m_e c\omega_{RF}$ [9] due to the maximum surface field allowed by breakdown [10]. The 3D model of this version of the device is shown in Fig. 5. In this case the ratio between the peak field at cathode and the average electric field inside the TW section is 4.1 and it is obtained using a coupling iris radius of 3 mm. As shown in Fig. 6, S_{11} at the waveguide input port

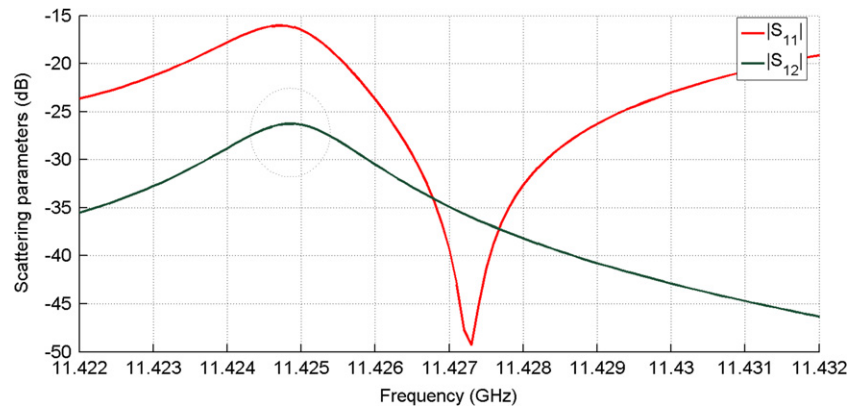


Fig. 6. S_{11} at the waveguide input port and S_{21} between the gun probe and the waveguide input port.

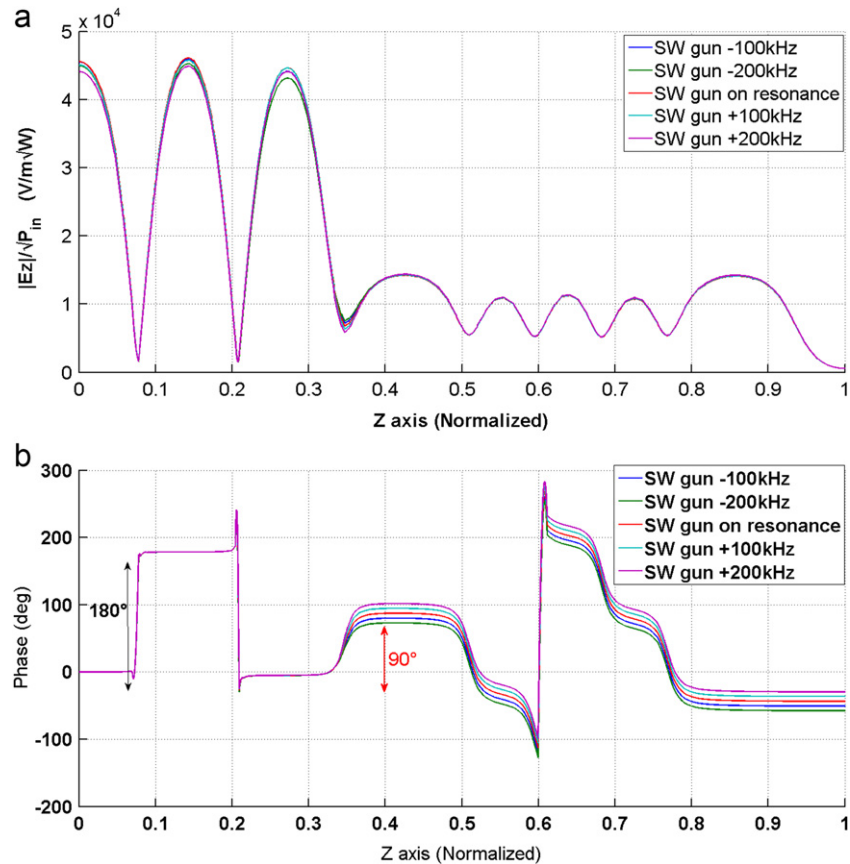


Fig. 7. Amplitude (a) and phase (b) of the electric field as a function of the longitudinal position for different resonant frequencies of the SW gun.

and S_{21} between the gun probe (that is an antenna in the SW part) and the waveguide input port are reported. The phase between the SW and the TW structures has a high sensitivity to the resonant frequency of the SW structure itself, as shown in Fig. 7 where the phase (b) of the electric field has been plotted for different resonant frequencies of the SW gun. In the same figure (a) the amplitude of the accelerating field is also given. Varying the frequency respect to the resonance we notice a variation of the phase difference between the standing and the traveling section of approximately 6° for a frequency sweep of 100 kHz. With good temperature control, considering that in X-band one could have 200 kHz/ $^\circ\text{C}$, it is possible to tune the phase difference between the SW and TW part of the hybrid gun optimizing the photoinjector performances during operation without notably changing the respective amplitudes of the accelerating field. In particular, with a temperature change of 1°C one can tune the relative phases by 12° , thus giving a degree of freedom in dynamics optimization.

3. Beam dynamics

From the beam dynamics point of view, as stated above, the simulation results obtained from a first optimization study on the hybrid structure are very promising and assuredly deserve further refinement. The peculiar property of this device is that it provides strong longitudinal focusing due to 90° phase shift between SW cell and input coupler and the emittance compensation dynamics remains manageable even in the presence of this strong compression. The velocity bunching concept is based on the property that if the beam is injected at the zero crossing field phase in the input coupler and it is slightly slower than the phase velocity of the RF wave, it will slip back to phases where the field is accelerating, but at the same time it will be chirped and compressed [11]. This feature makes the hybrid photoinjector suitable for a large variety of applications, in particular for applications that require very short pulse electron beams [3]. As already pointed out, the design strategy of the X-band hybrid photoinjector started with scaling the S-band model to X-band, but practical limits require a

particular attention in both RF and magnetostatic designs. It is necessary to utilize a different design for an appropriate solenoid configuration because the magnetic field reaches a peak value of 6 kG, whereas in the S-band case it has an easily manageable value of 1.5 kG. Moreover the peak of the electric field at the cathode obtained through use of the scaling law is 240 MV/m, but we limited this value to 200 MV/m due to RF breakdown considerations [10], as noted above. The beam dynamics simulations are performed by using PARMELA [12]. Here we report the simulation results obtained by considering the 2.6 SW gun model. Due to requirements of the applications of interest, it was necessary to increase the gun cells in order to achieve an energy level of 3.5 MeV at the gun exit. The distribution of the input beam is uniform and rectangular in both the radial and longitudinal direction. We can control two parameters: laser injection phase and the gun solenoid field. We can also vary the initial bunch distribution and charge. The initial radius is 0.07 mm, the length 0.5 ps, the charge 6.75 pC, and the initial normalized emittance of 0.008 mm-mrad. The amplitude of the $E_{z,p,SW}/\langle E_{z,TW} \rangle$ accelerating fields, the solenoid field in the SW and TW structures ($B_{z,SW}$, $B_{z,TW}$) and the laser input phase are optimized to maximize the brilliance of the beam at the end of the structure. The results of preliminary simulations in terms of beam energy, bunch length, rms beam envelope and normalized emittance along the structure are shown in Fig. 8 (red curves). The beam is focused by the first solenoid and its size is maintained under the field of the downstream magnets. The bunch length is initially increased by space charge force. Soon after the beam enters into the TW section, it begins to bunch. The rms bunch length reaches a minimum value of $5\ \mu\text{m}$ (16 fs), with a peak current of $165\ \text{A}$ at a distance of 30 cm from the cathode. The rms normalized emittance is near 0.08 mm-mrad. With this combination of extreme short pulse and low emittance, the brightness of this beam is remarkable: it is approximately a hundred times higher than the LCLS photoinjector beam after compensation. These values refer to the case of injecting the beam at 30° with respect to the zero of the RF field. Earlier injection times produce stronger compression. Since the over-bunching in this case

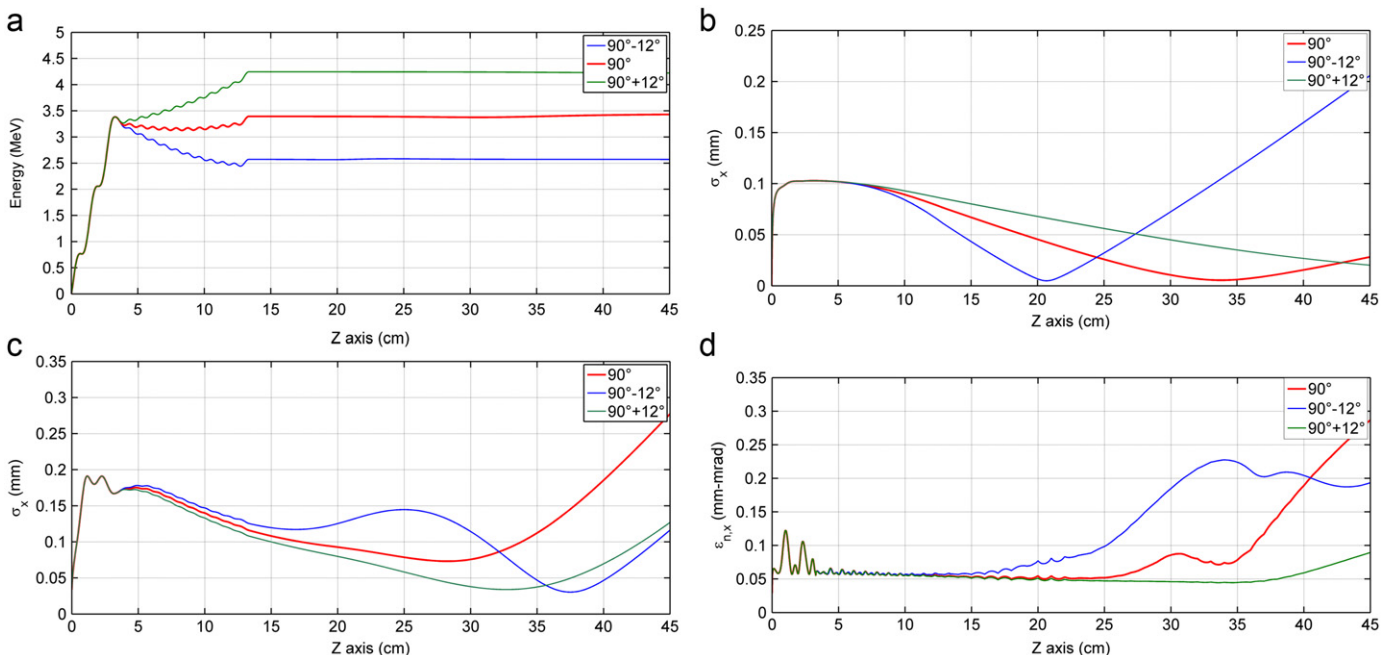


Fig. 8. Evolution of beam energy (a), rms bunch length (b), transverse beam size (c), normalized emittance and (d) for a beam charge of 6.75 pC. The red, blue and green lines represent, respectively, the cases of a phase difference between the SW section and the input coupler of 90° , 78° , 102° . (For interpretation of the references to colour in this figure legend, the reader is referred to the web version of this article.)

worsens the emittance, it is safe to inject slightly later than the shortest timing that is at about 28° . As explained above, although the phase between the last standing wave cell and the input coupler is nominally 90° , it is possible to tune this phase with a temperature variation. In particular one may exploit this phase adjustment to conveniently control acceleration and compression of the beam. In this way, starting with the results above presented, considering for example a variation of 1°C (and opportunely adjusting the timing of photocathode drive laser injection), i.e. a relative phase difference of

$+12^\circ$, one may continuously accelerate the beam to boost the output energy level to 5 MeV preserving a good level of the beam compression and emittance. On the other hand, one can have longitudinally focus beams at different distance from the cathode tuning of the relative SW-TW phase to $<90^\circ$ (See Fig. 8).

4. RF Measurements

To test the RF performance of the X-band hybrid and the manufacturing process, a cold test model was fabricated. The hybrid cold test model is a copper device with 3 ports designed to include two periods in the travelling wave section, i.e. six cells; the SW part has 1.6 cell, as the device shown in Figs. 1 and 2. The device, shown in Fig. 9, thus contains 10 total cells (two standing wave cells, six travelling wave cells and input and output couplers), its total length being 11.7 cm.

The non-resonant perturbation method by to Steele [13] is used for measurements in both the standing wave and travelling wave sections. The more common Slater method for cavity measurements is inadequate for non-resonant devices while Steele method can be used for both resonant and non-resonant volumes [14], and it is thus optimum for measuring the hybrid structure. In order to apply the Steele method to both SW and TW systems without perturbing the measurements it is advisable to use an extremely small bead, and, for example, a small drop of glue is enough to get reliable measurement in X-band devices.

The present bead pull system consists of a simple weight and a stepper motor system, which rotates, pulls the bead through the device under test (DUT); all the measurements are made using a vector network analyzer since the phase information is also needed. In order to properly measure the electric field on-axis,

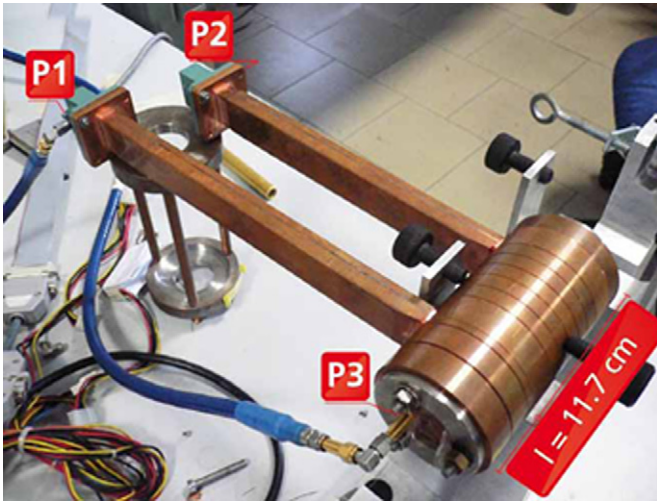


Fig. 9. Device under test. The hybrid photoinjector is a three ports structure. Port 1 and 2 are, respectively, the input and output ports connected to two rectangular waveguides, port 3 is accessible through a antenna.

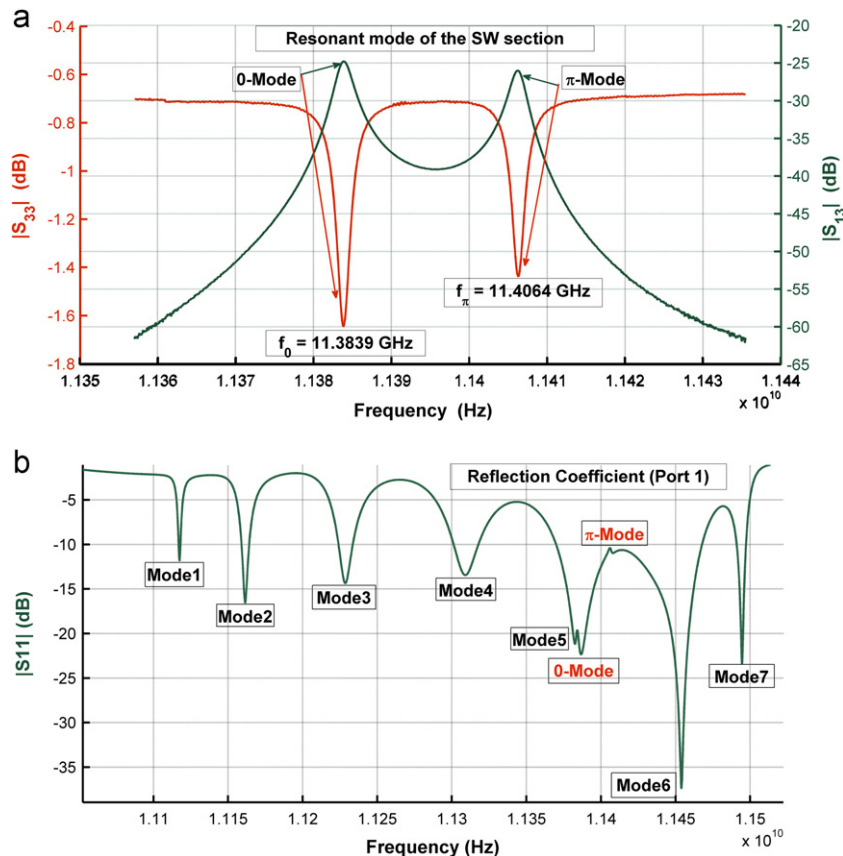


Fig. 10. Resonant modes of the standing gun (a) and reflection coefficient at port 1 (b).

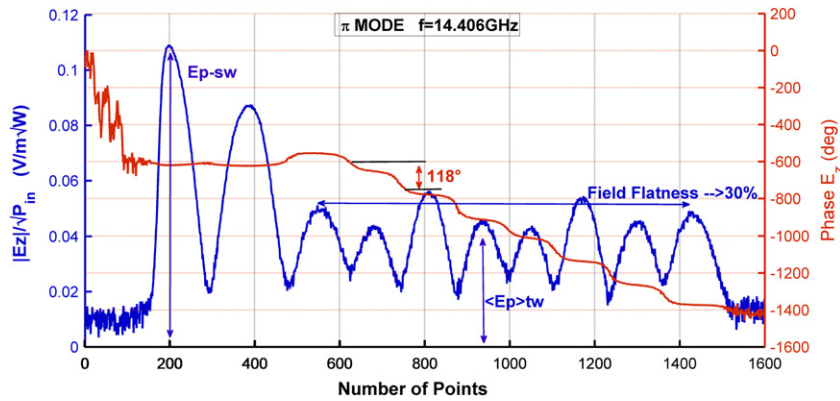


Fig. 11. Amplitude and phase of the measured electric field using bead pull technique.

the measurement must be made at the correct frequency, *i.e.* at the frequency, in which the field in the SW sub-structure is maximum. The resonant frequencies of the gun are visible on the S_{13} curve shown in Fig. 10, which also reports the reflection coefficient at the gun port (*i.e.* port 3). The two modes 0 and π of the SW part are at $f_0 = 11.3839$ GHz and $f_\pi = 11.4064$ GHz. Looking at the reflection coefficient at port 1 shown in Fig. 10, small deflections are present in correspondence of f_0 and f_π because of the RF filling of the SW section.

The travelling section is theoretically designed to work with $2\pi/3$ phase shift at 11.424 GHz and this frequency has to be matched with the π -mode frequency of the SW cavity. By measuring the reflection coefficient at port 1, one may have a constant phase shift of 240° (according to Steele method, the S_{11} parameter experiences a phase difference that is twice the phase of the electric field) but at a frequency different from the one corresponding to the complete filling of the SW part.

As shown in Fig. 11 the measured amplitude of the electric field normalized to the square root of the incident power and the phase is shown. At the resonant frequency of the gun, looking at the phase advance per cell, one can note that the key feature of a $\pi/2$ phase advance between the standing wave and travelling wave sections is evident.

We now compare measurements and simulations. Unlike simulations, the resonant frequency of the SW section does not match the frequency of the $2\pi/3$ -mode and therefore we do not observe a phase advance of 120° (118°) in the travelling wave section. Optimization of this aspect requires the realization of a tuning system in order to achieve the perfect matching between the two modes. Another important difference in comparison with simulations is the ratio $E_{z,p,SW}/\langle E_{z,TW} \rangle$; the measured one is approximately 2 instead of the design value of near 4. We can attribute these disagreements to an imperfect mechanical realization of the prototype and probably, looking at the reflection coefficient at port 1, to inadequate accuracy in the dimensions of the couplers to the two waveguides at port 1 and 2.

Moreover, it is also important to underline that the measured prototype needs tuning and the DUT is not brazed; this last aspect could partially result in a lower field in the SW part and therefore a lower ratio $E_{z,p,SW}/\langle E_{z,TW} \rangle$. Nevertheless, the non-perfect RF contacts can explain only partially the difference between measurements and simulations since the measured and simulated quality factors (*i.e.* $Q_{HFSS} = 6081$ and $Q_{meas} = 5460$, respectively) are relatively close. In all likelihood, the disagreement between the design and the measured ratio $E_{z,p,SW}/\langle E_{z,TW} \rangle$ is due in part to brazing errors, and in part to an imperfect mechanical realization of the coupling iris dimension between the SW gun and the

coupler. However we can conclude that despite these effects, the measured field amplitude and phase are qualitatively in good agreement with the simulations.

5. Conclusion

We have illustrated the electromagnetic and beam dynamics design procedure of a new class of photoinjectors, consisting of hybrid standing/travelling wave structures that bring several advantages in RF and beam performance compared to conventional systems. This design has characteristics that make it scalable to X-band where the use of higher field amplitudes, particularly at the cathode, may be exploited to obtain high brightness electron beams. A paper dedicated to the applications enabled by this novel photoinjector can be found in Ref. [3].

Acknowledgments

The authors acknowledge useful discussions with S. Tantawi, G. D'Auria, A. Murokh and M. Ferrario. This work is supported in part by the U.S. Department of Energy Divisions of High Energy Physics and Basic Energy Sciences under Contracts nos. DE-FG02-07ER46272 and DE-FG03-92ER40693, the Office of Naval Research under Contract no. ONR N00014-06-1-0925, and by Committee V of the INFN-LNF-Italy.

References

- [1a] A. Fukasawa, et al., in: Proceedings of the Particle Accelerator Conference, Albuquerque, New Mexico, USA, THPAS052, 2007.
- [1b] J.B. Rosenzweig, et al., AIP Conf. Proc. 877 (2006) 635.
- [2] J.B. Rosenzweig, E. Colby, in: Proceedings of the AIP Conference 335; Advance Accelerator Concepts, 724, 1995.
- [3] J.B. Rosenzweig, et al., Nucl. Instr. and Meth. A, in this issue.
- [4] <http://www.ansoft.com/products/hf/hfss/>.
- [5] D. Alesini, et al., Nucl. Instr. and Meth. A 580 (2007) 1176.
- [6] H.A. Bethe, Phys. Rev. 66 (1944) 163.
- [7] R.E. Collin, Foundations for Microwave Engineering, McGraw-Hill, Inc., New York, 1992.
- [8] G. Botta, Studio analitico dei campi elettromagnetici in un fotoiniettore ibrido in banda X, Tesi di Laurea, University of Rome, Sapienza, 2006.
- [9] K.J. Kim, Nucl. Instr. and Meth. A 275 (1989) 201.
- [10] V.A. Dolgashev, et al., Status of high power tests of normal conducting single-cell standing wave structures.
- [11] L. Serafini et al., in: Proceedings of the AIP Conference 581, 87, Karpacz, Poland, 2001.
- [12] <http://laacg1.lanl.gov/>.
- [13] C.W. Steele, IEEE Trans. Microwave Theory and Tech. 14 (2) (1966) 70.
- [14] A. Mostacci, et al., in: Proceedings of the Particle Accelerator Conference, Vancouver, Canada, TH5PP086, 2009.